UNIVERSITY OF READING

Department of Mathematics

Modelling water uptake in rice using moving meshes

Juri Parrinello

August 2008

This dissertation is submitted to the Department of Mathematics in partial fulfilment of the requirement for the degree of Master of Science

Abstract

In this disseration a moving mesh method, based on a conservation of mass principle is used to obtain numerical approximations to the solutions of a non-linear diffusion equation. Non-linear diffusion is used to model water uptake in rice grains. The moving mesh method is adopted to reproduce the expansion of the kernel due to the presence of water absorption.

I confirm that this is my own work, and the use of all material from other sources has been properly and fully acknowledged.

Acknowledgements

I would like to thank my supervisor, Professor Mike Baines for his much appreciated help, enthusiasm and endless patience during the making of this dissertation.

Special thanks to the wonderful people I have met during my time in Reading. Finally, I wish to express my gratitude to the EPSRC for the financial support.

Contents

List of Figures

Chapter 1

Introduction

The use of adaptive mesh techniques in the solution of partial differential equations has become very popular, in particular, in problems where large variations occur locally in the solution. The main types of grid adaptation are: the *h*-refinement, which adds or removes nodes from the existing grid; the *p*-refinement, which modify the order of the polynomial used in the approximation according to the smoothness of the solutions, and the *r*-refinement, which relocates the nodes where needed. The latter is also known as a moving mesh method.

In this dissertation we will make use of a particular moving mesh finite element method based on the conservation of a distributed mass. The method is applied, in two dimensions, to a non-linear diffusion equation with variable diffusivity and a moving boundary.

Chapter 2 provides a succint introduction about rice in terms of origin, physical characteristics. The concept of moisture content is also mentioned in this chapter as part of the standard parameters specified by the law for good quality rice.

Chapter 3 gives an insight into the physical and chemical reactions behind the process of water uptake in a rice kernel while considering how researchers have used this knowledge to model diffusion and expansion.

Chapter 4 gives a brief account on moving mesh methods and mainly concentrates on the formulation of a specific method that will be used in the solution of the moving boundary problem studied here.

Chapter 5 states the assumptions upon which the model is based and gives the formulation of the problem, using the method introduced in the previous chapter. The coe□cient of di□usion and the initial reference grid are also defined and determined.

Chapter 6 provides the reader with the numerical results of the modelling work while checking the sensitivity of the model to the di□usivity parameter. Chapter 7 takes the role of the ending chapter thus reporting on conclusions and further work.

Chapter 2

Rice: a brief overview

Rice, a common name for about nineteen species of annual herbs of the grass family, is native to south-eastern Asia. Evidence of cultivation has been found in China and Thailand dating from about 6000 BC [1]. Rice is one of the major commercial cereal grains worldwide, along with wheat and corn. Over 90% of rice is produced and consumed in Asia. Rice is used on its own or in the preparation of numerous food items such as breakfast cereals, snack foods, desserts, and pre-cooked meals. In Asia, when beer is brewed, rice is traditionally used as an adjunct to provide additional sugars for the fermentation process because it is less expensive and readily available compared to cane sugar [2]. In Japan, rice (*Yamadanishiki* variety) is also used for brewing the japanese traditional rice wine, sake [3].

2.1 Botany

Rice is a cereal crop, a member of the grass family, *Graminae*. This family is divided into a number of genera or subfamilies, one of which is *Oryza*. This genus is further divided into a number of sections, one of

which is *Sativae*. There is a further subdivision into a series, the most relevant of which are: *Oryza sativa* and *Oryza glaberrima*. *Oryza sativa* is the world's most widespread series because it is used for human consumption. *Oryza glaberrima*, although used as human food, is grown only in Africa on a very small scale. The three most common subseries of *Oryza sativa* are: Japonica, Javanica, and Indica. Japonica varieties are mainly found in Japan and Korea. Javanica varieties are commonly found in Indonesia and the Philippines. Indica varieties are the majority of rice grown all over Asia including India. Some Indica varieties were also brought to America for large scale production. Needless to say, Indica are the world's staple food [4].

2.2 Grain structure

The anatomy of mature rough rice (complete grains with husks intact) consists of a brown kernel enclosed by the husk. The brown rice grain consists of bran layers, a germ and the starchy centre of the grain. The gross structure of the grain is shown in figure 2.1. The image has been taken from the British Nutrition Foundation website [5].

Figure 2.1: Structure of a mature rough rice grain.

The most visible part of a rough rice grain is the husk also known as the

hull. The hull is the outer layer covering the caryopsis and, although inedible, it makes up about 20 – 25% of the total grain weight. The hull serves as a protective barrier against insect infestation and environmental fluctuations. The caryopsis consists of three fibrous bran tissues: pericarp, tegmen and aleurone. Endosperm and embryo are also component parts of the caryopsis. The bran portion accounts for one tenth of the weight of the rough grain and has a high nutritional value because it contains proteins and lipids. The pericarp is made of thin bran layers of proteins. The tegmen consists of arrays of fatty materials. The aleurone surrounds the endosperm and the embryo. Its tissues are rich in protein and cellulose. The embryo is the reproductive organ of the grain and is very rich in protein and fat. The endosperm, the largest component of the grain, is mainly composed of starch granules, with minute amounts of proteins, lipids and water [6].

2.3 Classification

Depending on the colour of the caryopsis, rice can be brown, red or black. White rice is usually obtained from brown rice by removing the bran layers through a process known as milling. The red and black varieties are less common and essentially only available in Thailand and the Philippines [7].

Rice is also classified as glutinous and non-glutinous according to the type of starch found in the endosperm. There are two types of starch, namely, amylose and amylopectin. Amylose consists primarily of linear chains of carbohydrates, whereas amylopectin has a more branching tree-like structure. The ratio of amylose to amylopectin strongly a□ects

the appearance as well as the cooking characteristics of the grain.

Glutinous rice, also known as waxy rice, has a white and opaque endosperm. Its starch consists almost entirely of amylopectin. When cooked, the grain usually loses its original shape and becomes very sticky.

Non-glutinous or non-waxy rice has a translucent appearance and contains amylose as well as amylopectin. The cooked grain tends to retain its shape and is less sticky [7].

If rice is classified as long grain, medium grain or short grain then the classification should be in accordance with one of the following specification:

- Option 1: kernel length/width ratio.
- Option 2: kernel length.
- Option 3: a combination of kernel length and length/width ratio.

The specification used for this modelling work is Option 1. The classification criteria shown in Table 2.1 refer to milled grains (white rice). Table 2.1 has been adapted from Codex Alimentarius Commission, 1990 [8].

Table 2.1: Rice classification

Grain Class	Length/Width Ratio
Long	3.0 or more
Medium	between 2.0 and 2.9
Short	1.9 or less

2.4 Moisture content

In describing the state of the grain the concept of moisture content, here and after denoted by c, will be used. c represents the amount of water present in the grain and is expressed as the ratio of the mass of water to the mass of grain. Lower moisture limits should be required for certain destinations in relation to the climate, duration of transport and storage. High moisture directly reduces the quality of rice because the grain has the tendency to mould or spoil. This is a critical factor as it has a bearing on the keeping properties of grain during storage and also on the milling quality and yield. The National Food Authority [8] set the following specification for the moisture content of the grain: c = 15% at most.

Chapter 3

The hydro-thermal process

The hydro-thermal processing of rice grain has become one of the most studied cases in the food industries worldwide [9]. One of the major driving forces behind such a widespread interest is the need for better preprocessing techniques, such that the finished product can be easily and very quickly prepared yet still retaining texture and taste similar to those of the freshly cooked rice. Hence, there is a great need for appropriate mathematical models that describe accurately the hydration and rehydration of rice grain during cooking. Control and optimization of rice grain cooking, therefore, requires an understanding of the physical and chemical reactions involved. Such processes are: heat transfer, water diffusion, swelling and gelatinization of the starch granules.

3.1 Heat conduction

Experimental work on the hydration of grains [10] and modelling work [11] concentrating on a single cereal grain have shown that the con-

account and the internal temperature can be taken to be the bulk temperature, i.e., the internal temperature of the grain is spatially uniform across the grain and equal to the water temperature [12].

3.2 Water diffusion

Water migration in solid foods has been described using the concept that water motion is driven by the gradient of water content. This

Earlier studies [19], on the absorption of liquid water in wheat, found that water motion in food materials is a diffusion controlled process. Syarief *et al* [20] presented the results of careful experiments on moisture uptake from various part of a corn grain, and fitted the experimental data to numerical solutions of a non-linear diffusion equation. The following equation was used to describe moisture uptake at a temperature of 40°C:

$$\frac{\partial c}{\partial t} = \nabla \cdot (D(c)\nabla c) \ , \tag{3.1}$$

where the diffusivity $D(c)$ was defined by the function

$$D \equiv D_0 e^{\delta c} \ , \tag{3.2}$$

with D_0 and δ being positive real constants. For floury and horny endosperms, the average value found was

$$D(c) = 1.5 \times 10^{-11} e^{8.6c} \ m^2 s^{-1} \ . \tag{3.3}$$

Equation (3.1) is the n-dimensional form of the second law of diffusion, also known as Fick's second law, with variable diffusion coefficient. Fick's laws of diffusion are explained in detail in Appendix A.

Later studies conducted by Suzuki *et al* [21] and McGowan *et al* [22] have also come to the conclusion that the diffusion coefficient strongly depends on moisture content. Furthermore, they noticed that diffusion is also affected by temperature and internal composition of the grain. In modelling the change of moisture distribution in japonica short grain rice, Takeuchi *et al* [18] used a slightly modified version of equation (3.3) which takes into account not only the moisture dependence, but, also the effect of changes in temperature by using a negative exponential

function of time.

The diffusion coefficient values reported by Bello *et al* [12] varied between 1.4×10^{-11} m^2s^{-1} and 9.36×10^{-11} m^2s^{-1} for temperature range between 25°C and 90°C. For parboiling of whole rice grain, Bakshi and Singh [23] found that diffusion coefficent varied between 10^{-11} and 10^{-9} m^2s^{-1} for temperatures between 50°C and 120°C. Using finite element analysis for non-linear water diffusion during soaking of white rice, Zhang *et al* [24] reported values for diffusivity decreasing from 1.78×10^{-10} m^2s^{-1} to 8.33×10^{-11} m^2s^{-1} as the moisture content rose from 13% to 50% at a constant temperature of 60°C.

As seen from the above mentioned literature, a variety of techniques have been adopted in order to parameterize the diffusion coefficient under soaking and/or cooking conditions. All these models are based on the solution of Fick's second law of diffusion but differ in the geometry used to describe the structure of the rice kernel. Analytic solutions of the diffusion equation have been obtained for different shapes: infinite plane sheet, infinite and finite cylinder, and sphere. Among these geometries, the cylinder is the shape that most closely resembles a milled glutinous rice grain [7].

3.3 Swelling and gelatinization

When a rice grain is soaked up in water at room temperature (around 25°C), the moisture content increases only slightly. Water is taken up by the starch granules and the associated swelling is almost equal to that of the water absorbed. The swelling of the grain is reversible

for temperatures below the gelatinization temperature, T_{gel}, and irreversible for temperatures above T_{gel} [22].

As rice contains about 90% starch, rice cooking is essentially the irreversible reaction, known as gelatinization, between starch and water at elevated temperatures. This reaction occurs over a narrow temperature range of about 10°C, centred around the temperature T_{gel}. The gelatinization temperature range reported in [2] was between 65°C and 75°C. An experimentally derived dependence of gelatinization temperature on moisture content shows that if moisture content is too low then gelatinization can not take place. Also, the higher the moisture content, the lower the temperature at which the reaction can occur [22]. T_{gel} is also strongly influenced by the size of starch granules, smaller granules gelatinize at higher temperatures, and by the proportion of amylose to amylopectin. Starch gelatinization has been found to follow first order kinetics [23]. The model proposed in this dissertation will account for the effects of gelatinization on water absorption but will not make use of the first law of kinetics.

Summing up, during the cooking of rice, starch granules absorb water and swell to accommodate the additional water as the heating continues. When the gelatinization temperature is reached, the granules burst (the cell walls of the granules break) and the starch turns viscous or gelatinized. In terms of water absorption this means that initially gelatinization increases the diffusivity and therefore the rate of water uptake. However, as the reaction continues the starch granules keep on swelling and this gradually reduces water migration into the grain. When the granules burst the viscosity of the starch becomes very high to the point that no further water diffusion is possible [6]. The effects

of gelatinization on diusion were investigated by Takeuchi *et al* [18]. They found that in the initial stage of rice cooking, rapid diusion is the dominant process. In the middle stage, the rate of water migration reduces and gelatinization prevails. In the terminal stage, the moisture uptake further reduces until it reaches an equilibrium value, or we could also say that, at this stage of the process, the driving force behind the diusion process can no longer overcome the resistance of the highly viscous medium (the gelatinized starch), hence, no further diusion takes place.

Chapter 4

Moving mesh methods

Adaptive mesh techniques play an essential role in improving the accuracy of the numerical solutions of many physical problems. Mesh adaptation is prefered to fixed mesh schemes when features such as boundary and interior layers, blow-up and moving interfaces are to be solved accurately.

Moving mesh methods require the generation of an appropriate mapping from a fixed mesh (regular domain) in the computational space, Ω_c, to an auxiliary domain in the physical space, Ω. By defining a suitable mapping, one can control the mesh properties required for the underlining applications. Let $\boldsymbol{x} = (x_1, ..., x_n)$ denote the variables in the physical domain Ω and $\boldsymbol{\xi} = (\xi_1, ..., \xi_n)$, the variables in the computational domain Ω_c. This mapping is then defined as a one-to-one

The location based methods are so called because they control directly the location of the mesh points, or more precisely, the mapping $x(\xi)$ from the auxiliary to the physical domain. A typical example of this group is the variational method which defines the mapping from the computational to the physical domain by minimizing a variational or functional form [25].

The velocity based methods seek to target directly the time derivative of the mapping $x_t(\xi)$ (the mesh velocity). Examples of velocity based methods are: the classical Lagrangian method, the moving finite element method, the deformation method, and the geometric conservation law method [25]. In this dissertation, only the moving finite element method based on conservation will be discussed in greater detail because this is the method used to solve the moving boundary problem. For more details on the velocity and the location based methods please refer to the relevant literature [25]. In the next two sections, we describe the moving mesh finite element algorithm proposed by Baines *et al* [27]. The method is used for the adaptive solution of time-dependent partial di□erential equations (PDEs) wiole/mm7(9(bleuoeasetl)1(op)uoealyai2a4.e)uoealy9d8-25fftion

on a time-dependent domain $\Omega(t)$. In equation (4.2) $u(\boldsymbol{x}, t)$ is defined in a fixed frame of reference with coordinate $\boldsymbol{x}$ at time t and L is a differential operator involving only space derivatives. Using a Lagrangian like formulation, $\bar{\boldsymbol{x}}$ is taken to be a moving coordinate. By suitably defining an invertible mapping between the fixed coordinates $\underline{a}$ and the moving coordinates $\underline{\bar{x}}$ the PDE (4.2) in the moving frame becomes

$$\dot{u} - \mathrm{v} \cdot \nabla u = Lu \,, \tag{4.3}$$

where

$$\mathrm{v} = \frac{d\bar{\boldsymbol{x}}}{dt} \,. \tag{4.4}$$

Now, let $\Omega(0)$ be a reference test volume in the fixed frame at time $t = 0$ and $\Omega(t$

w is introduced, where w moves with the velocity $\dot{x}$ and satisfies the advection equation

$$\frac{\partial w}{\partial t} + \mathbf{v} \cdot \nabla w = 0 \,. \tag{4.7}$$

Applying the Reynolds Transport Theorem again gives the following general form of equation (4.5):

$$\begin{aligned} \frac{d}{dt} \int_{\Omega(t)} wu \, d\Omega &= \int_{\Omega(t)} (wu) \, d\Omega + \int_{\partial\Omega(t)} wu\mathbf{v} \cdot \mathbf{n} \, ds \\ &= \int_{\Omega(t)} w\frac{\partial u}{\partial t} + u\frac{\partial w}{\partial t} + \nabla(wu\mathbf{v}) \, d\Omega \,. \end{aligned} \tag{4.8}$$

Using the property in equation (4.7) the weak form of the PDE in the moving frame is

$$\frac{d}{dt} \int_{\Omega(t)} wu \, d\Omega - \int_{\Omega(t)} w\nabla \cdot (u\mathbf{v}) \, d\Omega = \int_{\Omega(t)} wLu \, d\Omega \,. \tag{4.9}$$

A distributed conservation principle is now introduced. The derivation of the moving coordinate system is based on this principle. A total mass $\theta(t)$ is defined by

$$\theta(t) = \int_{\Omega(t)} u \, d\Omega \,, \tag{4.10}$$

where the test volume $\Omega(t)$ is the entire spatial domain of the problem at time t, moving with velocity $\mathbf{v}$. The velocity of the moving frame is obtained by the weak form of the conservation principle

$$\int_{\Omega(t)} wu \, d\Omega = \lambda\theta(t) \,, \tag{4.11}$$

where w is a test function advected with velocity $\dot{x}$ which satisfies equation (4.7) and $\int w = 1$. The constant λ is determined by w and the initial data. The integral equation (4.11) depends on $\theta(t)$ and the

moving coordinate system. Differentiating (4.11) with respect to time gives

$$\frac{d}{dt}\int_{\Omega(t)} wu \, d\Omega = \lambda \frac{d\theta}{dt} = \lambda \dot{\theta}(t) \, . \tag{4.12}$$

Therefore, the weak form of the PDE in equation (4.9) becomes

$$\lambda \dot{\theta}(t) - \int_{\Omega(t)} w \nabla \cdot (u\mathbf{v}) \, d\Omega = \int_{\Omega(t)} wLu \, d\Omega \, , \tag{4.13}$$

and using integration by parts gives

$$\lambda \dot{\theta}(t) - \int_{\partial\Omega(t)} wu\mathbf{v} \cdot \mathbf{n} \, ds + \int_{\Omega(t)} u\mathbf{v} \cdot \nabla w \, d\Omega = \int_{\Omega(t)} wLu \, d\Omega \, . \tag{4.14}$$

In order to determine $\mathbf{v}$ uniquely, additional conditions are required on the mesh velocity. If the vorticity together with suitable boundary conditions are specified then, given $\dot{\theta}$ and u, the velocity can be uniquely determined. Suppose that the vorticity is zero so that $\nabla \times \mathbf{v} = 0$, then there exists the velocity potential ψ, so that

$$\mathbf{v} = \nabla$$

As in equation (4.16), $\dot{\theta}(t)$ is determined by differentiating equation (4.10) with respect to time and using the identity in equation (4.6), (or by summing (4.16) over w and using $\sum w = 1$), thus giving

$$\dot{\theta}(t) - \int_{\partial\Omega(t)} u\nabla\psi \cdot \mathrm{n}\, ds = \int_{\Omega(t)} (Lu + \nabla\cdot(u\nabla\psi))\, d\Omega\,, \qquad (4.18)$$

which can be evaluated in terms of ψ when u is known. In practice, equations (4.16) and (4.18) are simultaneously solved for ψ and $\dot{\theta}$.

4.2 The finite element formulation

The moving grid finite element algorithm is constructed using the weak forms derived in the previous section. The algorithm consists of the discrete forms of equations (4.11), (4.16), (4.17) and (4.18). In order to formulate these equations in the finite element form, we define the discrete equivalent of w to be φ_i (usual hat function) on a mesh $\boldsymbol{X}_i(t)$. Therefore, the required discrete forms are

$$\int_{\Omega(t)} \varphi_i u\, d\Omega = \lambda_i \theta(t)\,, \qquad (4.19)$$

$$\lambda_i\dot{\theta}(t) - \int_{\partial\Omega(t)} \varphi_i u\nabla\psi\cdot\mathrm{n}\, ds + \int_{\Omega(t)} u\nabla\psi\cdot\nabla\varphi_i\, d\Omega = \int_{\Omega(t)} \varphi_i Lu\, d\Omega\,, \quad (4.20)$$

$$\int_{\Omega(t)} \varphi_i \mathrm{v}\, d\Omega = \int_{\Omega(t)} \varphi_i \nabla\psi\, d\Omega\,, \qquad (4.21)$$

and

$$\dot{\theta}(t) - \int_{\partial\Omega(t)} u\nabla\psi \cdot \mathrm{n}\, ds = \int_{\Omega(t)} (Lu + \nabla \cdot (u\nabla\psi))\, d\Omega\,, \qquad (4.22)$$

where $u = \sum_i u_i\varphi_i$ and $\psi = \sum_i \psi_i\varphi_i$, for $i = 1, ..., N$.

The algorithm can be expressed as the solution of the following system of ordinary differential equations:

$$\frac{d}{dt}\begin{bmatrix} \vec{X} \\ \theta \end{bmatrix} = \vec{F}\,(\vec{X}, \theta)\,, \qquad (4.23)$$

where $\vec{X} = (X_1, ..., X_N)^T$. The sequence used to evaluate $\vec{F}\,(\vec{X}, \theta)$ will be omitted in this section. However, the sequence described in the work of Baines *et al* [27] will be used in the next chapter to solve the moving boundary problem.

Chapter 5

The mathematical model

The method used in this chapter is based on the conservation of the proportion within each computational patch, of the total integral of the mass of water, over the considered domain. The method returns the velocities of the mesh nodes, which move so that the conservation principle is satisfied within each patch. The velocities are determined by differentiating the conservation principle with respect to time. The new mesh points are then generated from the velocities using a time stepping algorithm.

5.1 Assumptions

In order to model water uptake in rice the following hypothesis were formulated:

1. The variety of rice used in this model is milled long grain Thai glutinous rice.

2. The grain is assumed to be a cylinder with radius $r = 1\ mm$ and total length $l = 6\ mm$.

in $\Omega(t)$ where $c = 0.15$ initially and

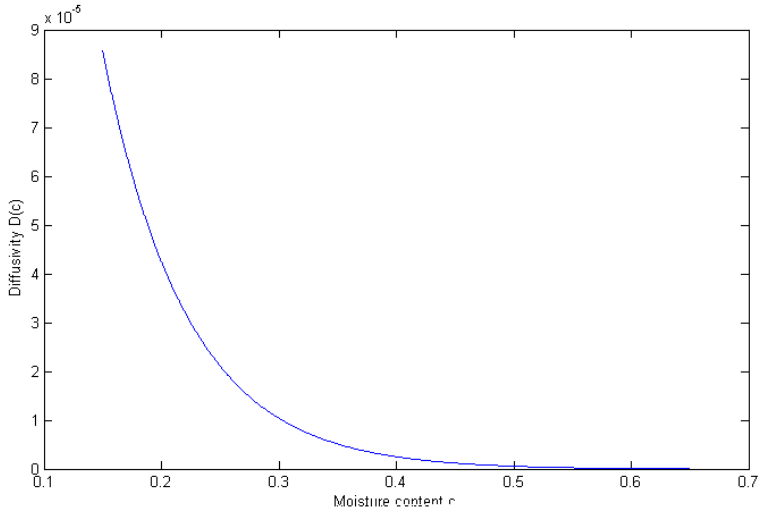

Figure 5.1: The diffusivity as function of moisture content.

Table 5.1: Diffusion coefficient

Moisture content c (%)	$D(c)$ $(mm^2 s^{-1})$
0.15	0.8564133×10^{-4}
0.20	0.4248888×10^{-4}
0.25	0.2106000×10^{-4}
0.30	0.1041873×10^{-4}
0.35	0.0513444×10^{-4}
0.40	0.0251034×10^{-4}
0.45	0.0120725×10^{-4}
0.50	0.0056015×10^{-4}
0.55	0.0023881×10^{-4}
0.60	0.0007924×10^{-4}
0.65	0.0000000×10^{-4}

5.3 Initial reference grid

We take a total of M nodes on each of the N concentric circles

$$0 = r_0 < r_1 < r_2 < \ldots < r_{N-1} < r_N = 1\,, \tag{5.4}$$

where the r's, representing the radii of the concentric circles, are equally spaced. The location of the nodes is chosen such that the nodes on r_0, r_2, r_4,... etc. correspond to even multiples of π/M and those on r_1, r_3, r_5,... etc. correspond to odd multiples of π/M.

The triangulation of the region is constructed using only two kinds of triangles: inward-pointing and outward-pointing isosceles triangles.

We choose $M = 107$ and $N = 20$. These values were obtained from the finite element project carried out as part of the MSc course and represent the optimal choice in terms of error minimization between the numerical approximation and the exact solution of a constant coe□cient Poisson equation. A simplified version of the initial reference grid is displayed in figure 5.2.

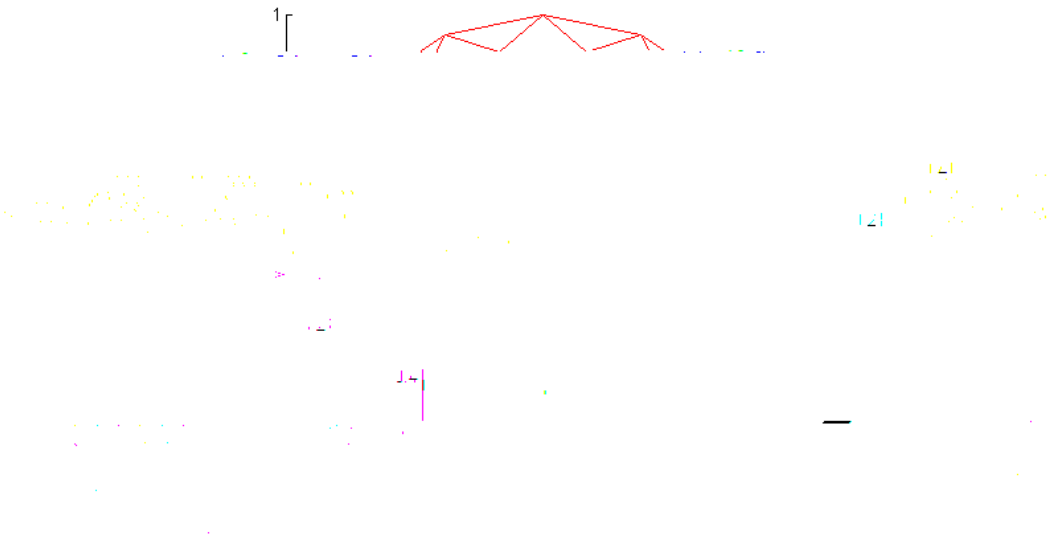

Figure 5.2: Example of an initial reference grid: 16 nodes, 8 circles.

The initial reference grid used in the model is shown in figure 5.3.

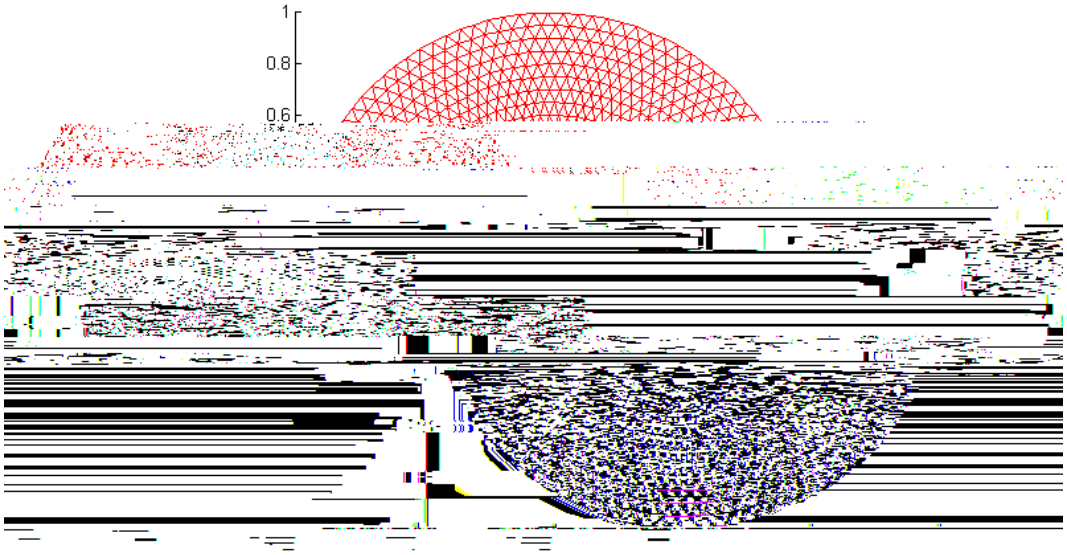

Figure 5.3: The initial reference grid: 107 nodes, 20 circles.

5.4 Formulation

Let's define the total integral of the water concentration to be

$$\theta(t) = \int_{\Omega(t)} c(x, y)\, d\Omega\,, \tag{5.5}$$

where

$$c = \sum_j c_j \varphi_j\,, \quad \text{for } j = 0, \ldots, N. \tag{5.6}$$

The φ's are the usual linear basis function in two dimensions.

Let the mesh move such that the distributed integral, or water fraction, is

where λ_i, which represents the water fraction for each patch$_i$, is fixed and equal to its value at $t = 0$, so that it can be precomputed. In fact

$$\lambda_i = \frac{\int_{\Omega(0)} \varphi_i c(0)\, d\Omega}{\int_{\Omega(0)} c(0)\, d\Omega} = \frac{0.15 \int_{\Omega(0)} \varphi_i\, d\Omega}{0.15 \int_{\Omega(0)} d\Omega}\,, \tag{5.8}$$

and given that φ_i is linear, (5.8) becomes

$$\lambda_i = \frac{1}{3}\frac{\text{Area of patch}_i}{\text{Total Area}} \quad [26]\,. \tag{5.9}$$

Note that $\sum_i \lambda_i = 1$.

Then using a weak form of the Reynolds Transport Theorem [27],

$$\begin{aligned} \frac{d}{dt}\int_{\Omega(t)} \varphi_i c\, d\Omega &= \int_{\Omega(t)} \{(\varphi_i c)_t + \nabla \cdot (\varphi_i c \mathbf{v})\}\, d\Omega \\ &= \int_{\Omega(t)} \varphi_i \{c_t + \nabla \cdot (c\mathbf{v})\}\, d\Omega \\ &= \lambda_i \dot{\theta}\,, \end{aligned} \tag{5.10}$$

where v

Integrating by parts,

$$\begin{aligned}\lambda_i \dot{\theta} &= \int_{\partial\Omega(t)} \varphi_i \, (D(c)\nabla c + c\mathbf{v}) \cdot \mathbf{n} \, ds \\ &\quad - \int_{\Omega(t)} \nabla\varphi_i \cdot \{D(c)\nabla c + c\mathbf{v}\} \, d\Omega \\ &= \int_{\partial\Omega(t)} \varphi_i \frac{\partial\psi}{\partial n} \, ds \\ &\quad - \int_{\Omega(t)} \nabla\varphi_i \cdot \{D(c)\nabla c + c\nabla\psi\} \, d\Omega \, , \qquad (5.12)\end{aligned}$$

since $\mathbf{v} = \nabla\psi$.

In each triangle, the diffusion coefficient is taken to be the average of the diffusivity at the three nodes

$$D(c) = \frac{1}{3} \left(D(c_1) + D(c_2) + D(c_3) \right) \, . \qquad (5.13)$$

There is no contribution from the internal boundaries in terms of φ's because $\varphi_i = 0$ there; however, the integral on the moving outer boundary is still there because of the jump in c, i.e., $D(c)\nabla c + [c]\,\mathbf{v} = 0$ with $c = 0.65$.

Expanding ψ in terms of the φ's as $\psi = \sum_j \psi_j \varphi_j$, the finite element matrix form, from (5.12), is

$$L \left. \frac{\partial\psi}{\partial n} \right|_{i=N\partial}$$

boundary to be $\psi_N = 0$, [27]. Therefore, equation (5.14) becomes

$$\frac{L}{h}\psi_{N-1}\underline{e}_N + K(c)\underline{\psi}_r + \dot{\theta}\underline{\lambda} = \underline{f}\,, \tag{5.16}$$

where h is the height of the triangle adjacent to the boundary, $K(c)$ is the weighted stiffness matrix with the last column removed, and $\underline{\psi}_r$ is a vector of the remaining ψ's. To solve equation (5.16) we use Schur's decomposition. Partition (5.16) as

$$\begin{bmatrix} K_r(c) & \underline{\lambda}_r \\ \underline{k}_N^T & \lambda_N \end{bmatrix} \begin{bmatrix} \underline{\psi}_r \\ \dot{\theta} \end{bmatrix} = \begin{bmatrix} \underline{f}_r \\ f_N \end{bmatrix}, \tag{5.17}$$

where $K_r(c)$ is the stiffness matrix with the last row and column removed, k_N^T is a vector of the first $N-1$ entries of the last row of $K(c)$ with the addition of the term L/h to the $(N-1)$'th entry. Inverting $K_r(c)$ formally in the first of (5.17),

$$\underline{\psi}_r = K_r(c)^{-1}(-\dot{\theta}\underline{\lambda}_r + \underline{f}_r)\,. \tag{5.18}$$

Substitu.0505.18)

Then, equations (5.20) and (5.18) become

$$\dot{\theta} = \frac{f_N - \underline{k}_N^T \underline{a}_r}{\lambda_N - \underline{k}_N^T \underline{b}_r} , \tag{5.22}$$

and

$$\underline{\psi}_r = -\dot{\theta}\underline{b}_r + \underline{a}_r , \tag{5.23}$$

To get the radial component v_i of $\mathbf{v}$, the velocities at the nodes, from ψ in the symmetric case we use

$$v_i = \left.\frac{\partial \psi}{\partial r}\right|_i , \tag{5.24}$$

in the upwind element where $r^2 = x^2 + y^2$. To obtain the new values for the nodal positions r_i^{n+1} and total integral of water concentration θ^{n+1}

Chapter 6

Numerical results

The numerical results presented here are compared with the experimental data reported in the work of Ahromrit [7]. The parameters were chosen in such a way as to match as accurately as possible the experimental results. The results reported in the following pages refer to grain moisture profiles over time, change of moisture content at the centre of the kernel versus time, grain volume increment and total volume of absorbed water.

The series of plots shown in figure 6.1 represent the moisture profile across half of the grain in the radial direction for different times t. As expected, as time goes by, the overall moisture profile increases until it reaches the equilibrium state at $c_e = 0.65$.

Figure 6.2 represents the increment of moisture at the centre of the grain as absorption takes place. This profile closely matches the experimental moisture profile reported in [7].

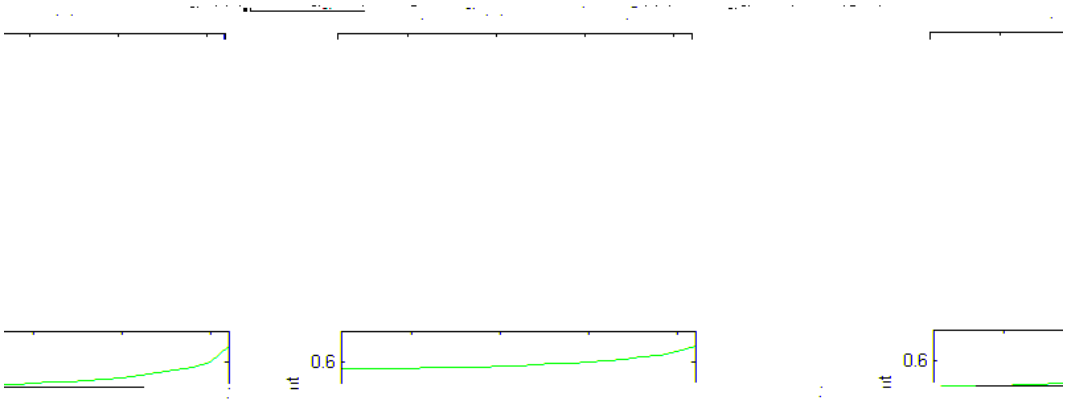

Figure 6.1: Moisture profile across the grain at di□erent times t.

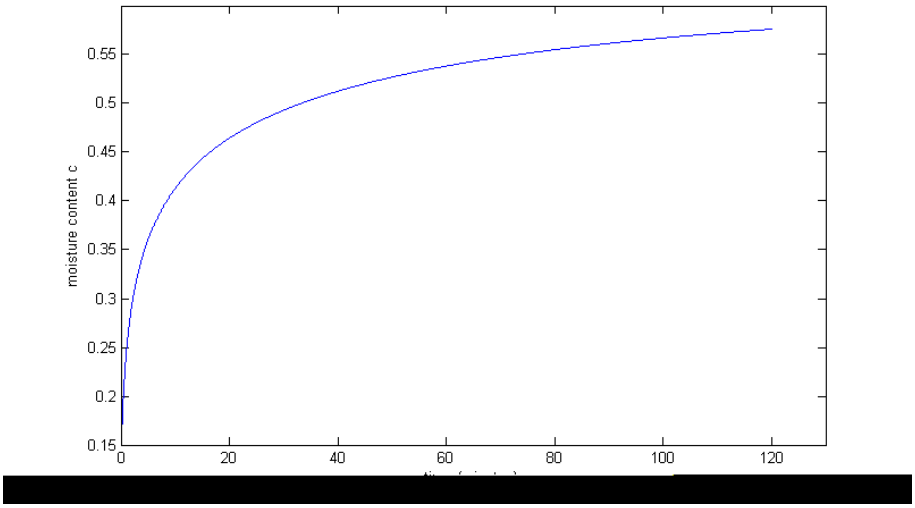

Figure 6.2: Increment in moisture content at the centre of the grain over time.

The volume at time $t = 0$ was given by

$$V_0 = \pi \times r^2 \times l = \pi \times 1^2 \times 6 = 18.85\ mm^2\ . \qquad (6.1)$$

The overall radial increment at the end of the process was found to be around 14% in accordance with the findings in Ahromrit [7]. Therefore, the volume of the grain at the end of the soaking period has increased as follows

$$V_{end} = \pi \times r^2 \times l = \pi \times 1.14^2 \times 6 = 24.50\ mm^2\ . \qquad (6.2)$$

The initial moisture content was set at $c = 0.15$. The moisture content at the end of the simulationm was found to be $c = 0.602$. It is clear then, that the overall volume increment of the kernel has not exactly reflected the total amount of water absorbed, which is, 60% of V_{end}. However, this has also been observed in Ahromrit [7] and it seems to be correct when considering that some of the water absorbed is filling the void spaces in the kernel.

More numerical results should have been presented in this work. Testing the sensitivity of the model on di□usivity and time steps would have been a further area of investigation. Reporting on water absorption rates, increments in radial expansion rates would have also benefit the overall value of my work. Unfortunately, I have simply run out of time and given my poor time managing skills, I was able to include very few numerical results.

Chapter 7

Conclusions

In this dissertation, a finite element moving mesh method based on a conservation of mass principle was implemented in order to obtain numerical approximations to the solution of a non-linear diffusion equation with variable diffusivity.

Water absorption kinetics was described using a model based on Fickian theory where the diffusion coefficient varied with exponential dependence on moisture content. The effects of temperature and major starch gelatinization were ignored and assumed not to be present given the choice of constant temperature. This choice was justified by the experimental results obtained by Ahromrit [7].

The size of the time step was also a limiting factor as pointed out in Chapter 5. A possible avenue for further work may consider the implementation of a more stable time stepping scheme. This in turn would benefit in terms of reduced computational time.

Further work could possibly look at the application of this moving mesh method to the three dimesional case. Also, the choice of more realistic diffusion coefficient should be looked at in more details.

Appendix A

Fick's laws of diffusion

Fick's laws of diffusion describe diffusion and can be used to solve for the diffusion coefficient D.

The first law is applied to steady state diffusion problems, i.e., when the concentration within the diffusion volume does not change with respect to time. The transfer of concentration per unit area in one-dimensional diffusion can be described by the following equation:

$$J = -D\frac{\partial c}{\partial t}, \tag{A.1}$$

biological molecules the diffusion coefficients normally range from 10^{-11} to 10^{-10} $m^2 s^{-1}$. In two or more dimensions equation (A.1) generalises as follows

$$J = -D\nabla c \, . \tag{A.2}$$

In chemical systems the driving force for diffusion of each species is the gradient of the chemical potential of this species. From the conservation of mass, we also know that:

$$\frac{\partial c}{\partial t} = -\frac{\partial J}{\partial x} \, . \tag{A.3}$$

Combining this relationship with the first law of diffusion, the second law of diffusion can be derived for the one-dimensional diffusion case:

$$\frac{\partial c}{\partial t} = D\frac{\partial^2 c}{\partial x^2} \, . \tag{A.4}$$

In equation (A.4) the diffusion coefficient has been assumed to be independent of concentration and time. This is not true for a number of food materials. The general form of the second law with variable diffusion coefficient for the one-dimensional case is:

$$\frac{\partial c}{\partial t} = \frac{\partial}{\partial x}\left[D\frac{\partial c}{\partial x} \right] \, . \tag{A.5}$$

In two or more dimensions equation (A.5) becomes

$$\frac{\partial c}{\partial t} = \nabla \cdot$$

Bibliography

[1] www.starch.dk/isi/starch/rice.htm, International Starch Institute: Rice, (last checked on 31.07.2008).

[2] M. J. Davey, K. A. Landman, M. J. McGuinness, H. N. Jing. Mathematical modeling of rice cooking and dissolution in beer production, *AIChE Journal*, 48, (8) (2002) 1811-1826

[3] A. K. Horigane, H. Takahashi, S. Maruyama, K. Ohtsubo, M. Yoshida. Water penetration into rice grains during soaking observed by gradient echo magnetic resonance imaging, *Journal of Cereal Science*, 44 (2006) 307-316

[4] www.teksengricemill.com, Knowledge about rice, (last checked on 27.07.2008).

[5] www.nutrition.org.uk/upload/ricegrain.gif, British Nutrition Foundation 2004, (last checked on 27.07.2008).

[6] C. R. Adair. Rice Chemistry and Technology, *D. F. Houston, St Paul*, 1972

[7] A. Ahromrit. High pressure induced water absorption characteristics of Thai glutinous rice, *PhD Thesis*, University of Reading, 2005

[8] www.fao.org/inpho/content/documents/vlibrary/t0567e/T0567E07.htm, Rice in human nutrition - Grain structure, composition and consumers' criteria for quality, (last checked on 27.07.2008).

[16] H. Watanabe, M. Fukuoka, A. Tomiya, T. Mihori. A new non-fickian di□usion model for water migration in starchy food during cooking, *Journal of Food Engineering*, 49 (2001) 1-6

[17] S. Takeuchi, M. Maeda, Y. Gomi, M. Fukuoka, H. Watanabe. An application of MRI to the real time measurement of the change

[24] T. Y. Zhang, A. S. Bakshi, R. J. Gustafson, D. B. Lund. Finite element analysis of non-linear water diffusion during soaking, *Journal of Food Science*, 49 (1984) 246-250

[25] W. Cao, W. Huang, R. D. Russell Approaches for generating moving adaptive meshes: location versus velocity, *Applied Numerical Mathematics*, 47 (2003) 121-138

[26] M. J. Baines. Lecture notes on finite element, *University of Reading*, 2008

[27] M. J. Baines, M. E. Hubbard, P. K. Jimack A moving mesh finite element algorithm for the adaptive solution of time-dependent partial differential equations with moving boundaries, *Applied Numerical Mathematics*, 54 (2005) 450-469

[28] H. C. Berg. Random Walks in Biology, *Princeton*, 1977